JCTC Journal of Chemical Theory and Computation

Article

pubs.acs.org/JCTC

Toward a Quantitative Assessment of Electronic Transitions' Charge-Transfer Character

Thibaud Etienne,*[,†,‡,§] Xavier Assfeld,[†,‡] and Antonio Monari[†,‡]

[†]Université de Lorraine − Nancy, Théorie-Modélisation-Simulation, SRSMC, Boulevard des Aiguillettes, 54506 Vandoeuvre-lès-Nancy, France

[‡]CNRS, Théorie-Modélisation-Simulation, SRSMC, Boulevard des Aiguillettes, 54506 Vandoeuvre-lès-Nancy, France

[§]Unité de Chimie Physique Théorique et Structurale, Université de Namur, Rue de Bruxelles 61, 5000 Namur, Belgium

Supporting Information

ABSTRACT: We hereby report studies devoted to a topological descriptor of photoinduced electronic charge density variation. Our novel index, symbolized as ϕ_S, consists in the detachment and attachment densities overlap, where the detachment density physically depicts the electron density removed from the ground state of a molecule during the transition while the attachment density consists in the rearranged density in the excited state. Our method provides a simple and efficient way to quantitatively evaluate how easy the charge-separation is made upon the chromophore's light absorption. Furthermore, this model can be applied for instance to address a comment on new push−pull dyes charge-transfer ability in order to assess their potentiality as candidates for light absorption-based devices. Moreover, the ϕ_S assessment allows us to perform some methodological diagnostic tests concerning the use of long-range corrected exchange−correlation functional in a time-dependent density functional theory (TDDFT) framework. This paper relates the ϕ_S descriptor's mathematical foundations from various perspectives (detachment/attachment densities or natural transition orbitals), together with its application to several types of chromophores. Connections and divergences with a formerly proposed index are finally evidenced.

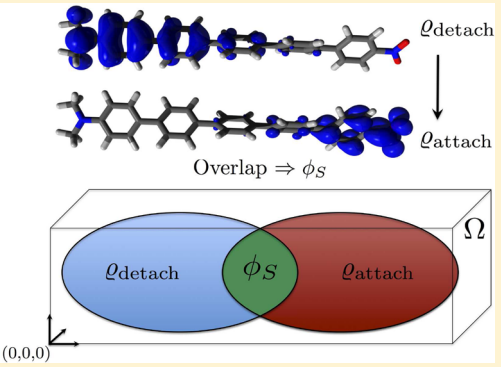

1. INTRODUCTION

Investigating a chromophore's electronic density reorganization upon light absorption is of seminal importance in the preliminar steps of molecular design of newly efficient photoactive systems and materials.[1−3] Indeed, if one has to discriminate among several sensitizers to build an original device, the knowledge of certain peculiar quantities related to photosensitization could lead for instance to probatory conditions, and hence to a rational classification of the potential candidates.[4−6] For instance, light-emitting diodes or dye-sensitized solar cells involve complex molecular systems, usually some conjugated donor−bridge−acceptor (D−π−A) dyes, which are usually designed to exhibit a low-energy light absorption profile and long-ranged intramolecular charge-transfer upon excitation.[7] A qualitative depiction of such electronic transition consists in representing the ground state chromophore as D−π−A and the excited state of interest as D^+−π−A^- to highlight the electronic cloud reorganization, although no net charge is actually held by the donor (acceptor) fragment in the excited state.

Charge-transfer transitions computation constitutes a methodological issue in the framework of time-dependent density functional theory (TDDFT). Indeed, the ability of an exchange−correlation functional to accurately reproduce the transition energies of a compound highly relies on whether the target transitions have a high charge-transfer character or not.[8,9] In the case of a long-range charge-separation, efficient corrections to the usual xc-functionals have already been implemented and validated. The need of a diagnostic tool to assess the charge-transfer character of an electronic transition was brought by Peach and Tozer,[10,11] who elaborated the λ index, whose value indicates whether a range-separated hybrid functional is required for an accurate computation of an electronic transition's energy.

The present article reports a new strategy for retrieving crucial topological information related to charge-transfer from the so-called detachment/attachment[12,13] density matrices and natural transition orbitals.[14−17] In particular, a novel descriptor, ϕ_S, is formally defined as the spatial overlap between detachment and attachment densities. We will show that the ϕ_S index allows us to quantitatively represent the charge-separation nature of a chromophore upon light absorption and hence constitutes a reliable diagnostic tool for xc-functionals. Multiple series of chromophores are investigated, so that we can compare their ϕ_S values with respect to the type of dye and the level of theory. More information is addressed in the Theoretical Background and Computational Details section.

Received: May 7, 2014
Published: July 23, 2014

   dx.doi.org/10.1021/ct5003994 | J. Chem. Theory Comput. 2014, 10, 3896−3905

Although ϕ_S is general and can be used for any quantum-chemical method, in this contribution, the excited states calculations are performed at the TDDFT level of theory. An alternate definition of ϕ_S will be brought out by pointing out the closeness of the physical meaning between detachment/attachment densities and natural transition orbitals (NTOs). NTOs have already been used for representing crucial topological features concerning electronic excitation of different chromophores.[18−25]

2. THEORETICAL BACKGROUND AND COMPUTATIONAL DETAILS

The first part of this section is devoted to the theoretical background related to the key tools that will be used throughout this article. The subsequent paragraph gives a detailed depiction of the calculations reported in the results section.

2.1. The ϕ_S Descriptor. From excited states quantum-chemical calculations of a N-electron system with a K-sized basis set, one obtains the basis set overlap matrix ($\mathbf{S}$), the density matrices corresponding to the ground state ($\mathbf{P}_0$) and to the X^{th} excited state ($\mathbf{P}_X$). It is thus possible to derive the $\mathbf{\Delta}$ matrix as the difference between excited $\mathbf{P}_X$ and ground state $\mathbf{P}_0$ density matrices

$$\Delta = \mathbf{P}_X - \mathbf{P}_0 \Rightarrow \sum_{k=1}^{K} (\mathbf{\Delta S})_{kk} = 0 \tag{1}$$

the trace of $\mathbf{\Delta S}$ being zero because no electron was gained or lost by the system. Performing an unitary similarity transformation on $\mathbf{\Delta}$ provides the eigenvalues of $\mathbf{\Delta}$ in the diagonal matrix $\boldsymbol{\delta}$

$$\exists\ \mathbf{U} \mid \boldsymbol{\delta} = \mathbf{U}^{\dagger}\mathbf{\Delta U};\ (\boldsymbol{\delta})_{ij} = 0 \quad \forall\ i \neq j \tag{2}$$

Note that by diagonalizing the $\mathbf{\Delta}$ matrix one obtains the so-called detachment/attachment orbitals.[16] The eigenvalues of $\mathbf{\Delta}$ are either positive or negative. We can now define two new diagonal matrices, σ_- and σ_+, whose components are functions of those from $\boldsymbol{\delta}$:

$$(\boldsymbol{\sigma}_{\pm})_{kj} = \frac{1}{2}\left(\sqrt{(\boldsymbol{\delta})_{kk}^2} \pm (\boldsymbol{\delta})_{kk}\right) \times \delta_{kj} \mid \boldsymbol{\delta} = \sum_{\omega=+,-} \omega\boldsymbol{\sigma}_{\omega} \tag{3}$$

where δ_{kj} is the Kronecker delta function and $(\boldsymbol{\delta})_{kk}$ is a component of the $\boldsymbol{\delta}$ matrix. The $\boldsymbol{\sigma}$ function splits $\mathbf{\Delta}$'s eigenvalues into two arrays: $\boldsymbol{\sigma}_-$ keeps the absolute value of negative $\boldsymbol{\delta}$ values and sets non-negative ones to zero. Conversely, $\boldsymbol{\sigma}_+$ contains only positive values from the $\boldsymbol{\delta}$ diagonal and zeros. Backtransforming $\boldsymbol{\delta}$, $\boldsymbol{\sigma}_-$, and $\boldsymbol{\sigma}_+$ gives

$$\left.\begin{aligned} \mathbf{\Delta} &= \mathbf{U}\delta\mathbf{U}^{\dagger} \\ \mathbf{\Gamma} &= \mathbf{U}\sigma\_\mathbf{U}^{\dagger} \\ \mathbf{\Lambda} &= \mathbf{U}\sigma_{+}\mathbf{U}^{\dagger} \end{aligned}\right\} \Rightarrow \mathbf{\Delta} = \mathbf{\Lambda} - \mathbf{\Gamma} \tag{4}$$

The two newly obtained matrices are the so-called detachment $\mathbf{\Gamma}$ and attachment $\mathbf{\Lambda}$ density matrices and are expressed in the space of the K atomic orbitals φ_μ. We see that

$$\sum_{\mu=1}^{K} (\mathbf{\Gamma S})_{\mu\mu} = \sum_{\mu=1}^{K} (\mathbf{\Lambda S})_{\mu\mu} \tag{5}$$

because no electron is lost during the excitation process. It is thus possible to define the related detachment/attachment densities in the real 3D space (ξ_1, ξ_2, and ξ_3 being the three spatial coordinates)

$$\varrho_{\boldsymbol{\tau}}(\xi_1, \xi_2, \xi_3) = \sum_{\mu=1}^{K}\sum_{\nu=1}^{K} (\tau)_{\mu\nu}\varphi_{\mu}(\xi_1, \xi_2, \xi_3)\varphi_{\nu}^{*}(\xi_1, \xi_2, \xi_3)$$
$$\boldsymbol{\tau} \equiv \mathbf{\Gamma}, \mathbf{\Lambda} \tag{6}$$

These two functions are actually representative of the spatial distribution of the electronic density removed (detachment) from the ground state and reorganized (attachment) in the excited one during the transition. Notably, we may define the detached/attached charge $\vartheta_{\boldsymbol{\tau}}$ as

$$\vartheta_{\boldsymbol{\tau}} = \int_{\mathbb{R}} \mathrm{d}\xi_1 \int_{\mathbb{R}} \mathrm{d}\xi_2 \int_{\mathbb{R}} \mathrm{d}\xi_3 \varrho_{\boldsymbol{\tau}}(\xi_1, \xi_2, \xi_3) \equiv \int_{\mathbb{R}^3} \mathrm{d}^3\xi\, \varrho_{\boldsymbol{\tau}}(\xi)$$
$$\boldsymbol{\tau} \equiv \mathbf{\Gamma}, \mathbf{\Lambda} \tag{7}$$

We would like to draw the reader's attention to the fact that the $\varrho_{\mathbf{\Gamma}}$ and $\varrho_{\mathbf{\Lambda}}$ density functions are different from those of Le Bahers et al.[41] (namely, ρ_- and ρ_+). Similarly, $\vartheta_{\mathbf{\Lambda}}$ is not identical to the q_{CT} transferred charge. Indeed, the detachment/attachment-related functions were obtained from a preliminary operation performed in the Hilbert space (in order to obtain the $\mathbf{\Gamma}$ and $\mathbf{\Lambda}$ density matrices), followed by a projection in the direct space, while the ρ functions were derived by taking directly the difference between excited and ground states density functions in the real space. Those differences are formally detailed in a distinct paper,[47] which is a companion to the present one.

We now define the dimensionless ϕ_S index as the overlap between the attachment and detachment densities

$$\phi_S = \vartheta^{-1} \int_{\mathbb{R}^3} \mathrm{d}^3\xi \sqrt{\varrho_{\mathbf{\Gamma}}(\xi)\varrho_{\mathbf{\Lambda}}(\xi)}$$
$$\vartheta \equiv \frac{1}{2}\left[\int_{\mathbb{R}^3} \mathrm{d}^3\xi \sum_{\boldsymbol{\tau}=\mathbf{\Gamma},\mathbf{\Lambda}} \varrho_{\boldsymbol{\tau}}(\xi)\right] \quad \phi_S \in [0;\ 1] \tag{8}$$

The ϕ_S index takes values ranging from 0 to 1, depending on the charge-transfer character of the electronic transition. The first possibility occurs when there is strictly no overlap between detachment and attachment densities. Conversely, the second bound value depicts the extreme case where the transition is so that there is a zero electronic density fluctuation between ground and excited states. Note that in practice one will consider a tridimensional integration grid surrounding the chromophore and will integrate the detachment/attachment densities over the delimited volume Ω as depicted in Figure 1.

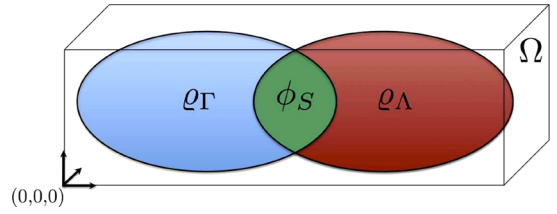

Figure 1. Graphical depiction of the ϕ_S descriptor as the overlap between detachment and attachment densities.

dx.doi.org/10.1021/ct5003994 | J. Chem. Theory Comput. 2014, 10, 3896−3905

An interesting property concerns calculations where no de-excitations are considered (i.e., within the Tamm−Dancoff approximation[26] or the CIS method). One formally obtains

$$\int_{\mathbb{R}^3} \mathrm{d}^3\xi \varrho_{\mathbf{\Gamma}}(\xi) = \int_{\mathbb{R}^3} \mathrm{d}^3\xi \varrho_{\Lambda}(\xi) = \sum_{k=1}^{K} (\mathbf{\Gamma S})_{kk} = \sum_{k=1}^{K} (\mathbf{\Lambda S})_{kk} = 1 \tag{9}$$

2.2. Natural Transition Orbitals Derivation of the ϕ_S Index. In addition to the difference density matrix, it is sometimes useful to characterize an electronic excited state by means of the so-called transition density matrix. We introduce the *one-particle reduced transition density projector* $\hat{\gamma}(\mathrm{x}_1,\mathrm{x}_1')$, where $\mathbf{x}$ collects spatial and spin coordinates

$$\hat{\gamma}(\mathrm{x}_1, \mathrm{x}_1') = N \int_{\mathrm{x}_2} \mathrm{dx}_2 \cdots \int_{\mathrm{x}_N} \mathrm{dx}_N |\mathbf{\Psi}_0(\mathrm{x}_1, \mathrm{x}_2, ..., \mathrm{x}_N)\rangle \times \langle \mathbf{\Psi}_{\mathrm{x}}(\mathrm{x}_1', \mathrm{x}_2, ..., \mathrm{x}_N)| \tag{10}$$

where we set conventionally for any $|\mathbf{\Psi}_s\rangle$ and $\langle \mathbf{\Psi}_r|$

$$\int_{\mathrm{x}_k} \mathrm{dx}_k |\mathbf{\Psi}_s\rangle\langle\Psi_r| \equiv \int \mathrm{dx}_k \langle \mathrm{x}_k|\mathbf{\Psi}_s\rangle\langle\mathbf{\Psi}_r|\mathrm{x}_k\rangle \tag{11}$$

$\hat{\gamma}(\mathrm{x}_1,\mathrm{x}_1')$ can be expressed in the basis of spin orbitals (Θ) by its matrix representation $\mathbf{T}$

$$(\mathbf{T})_{mn} = \langle \Theta_m(\mathrm{x}_1)|\hat{\gamma}(\mathrm{x}_1, \mathrm{x}_1')|\Theta_p(\mathrm{x}_1')\rangle \quad m \subset \{1, N\} \quad n \subset \{1, K-N\} \quad (p = N + n) \tag{12}$$

One can easily show that if the excited state is expressed as an expansion in the space of monoexcited Slater determinants, $\hat{\gamma}(\mathrm{x}_1,\mathrm{x}_1')$ reduces to

$$\hat{\gamma}(\mathrm{x}_1, \mathrm{x}_1') = \sum_{i=1}^{N} \sum_{a=N+1}^{K} c_i^a |\Theta_i(\mathrm{x}_1)\rangle\langle\Theta_a(\mathrm{x}_1')| \tag{13}$$

leading to

$$(\mathbf{T})_{mn} = \sum_{i=1}^{N} \sum_{a=N+1}^{K} c_i^a \langle \Theta_m(\mathrm{x}_1)|\Theta_i(\mathrm{x}_1)\rangle\langle\Theta_a(\mathrm{x}_1')|\Theta_p(\mathrm{x}_1')\rangle = \sum_{i=1}^{N} \sum_{a=N+1}^{K} c_i^a \delta_{im}\delta_{ap} = c_m^p \tag{14}$$

where c_m^p is the coefficient weighting the monoexcitation from the m^{th} to the p^{th} spin orbital involved in the transition from the ground to the X^{th} state. These coefficients are stored in the rectangular $N \times (K - N)$ transition density matrix $\mathbf{T}$, with c_m^p being the $(\mathbf{T})_{mn}$ coefficient, with $n = p - N$.

One can further perform a singular value decomposition[27] (SVD) of the rectangular transition density matrix $\mathbf{T}$ into $\mathbf{X}$ and hence obtains the so-called natural transition orbitals (NTOs) rotation matrices

$$\mathbf{X} = \mathbf{O}^\dagger\mathbf{T}\mathbf{V} \quad (\mathbf{X})_{ij} = x_i\delta_{ij} \tag{15}$$

where the $N \times (K - N)$ $\mathbf{X}$ matrix's diagonal contains the singular values, i.e., the descending-ordered relative weights of the couples of occupied (ψ_k^{o}) and virtual (ψ_k^{v}) natural transition orbitals involved in the electronic transition. $\mathbf{O}$ and $\mathbf{V}$ matrices are $(N \times N)$ and $([K - N] \times [K - N])$ sized and store the occupied and virtual NTOs coefficients, respectively (see below). Thus, instead of describing one excitation with multiple canonical spin orbitals couples, one usually gathers all the physical information on the nature of the electronic transition in one (sometimes two) couple(s) of NTOs. More details on the obtention of the $\mathbf{X}$ rectangular matrix by SVD are addressed in Appendix B.

As mentioned in the introduction, we can derive ϕ_S also from the natural transition orbitals formalism. We start with the NTOs definition with respect to canonical spin orbitals

$$\psi_k^{\mathrm{o}} = \sum_{i=1}^{N} (\mathbf{O})_{ik}\mathbf{c}^i \quad \psi_k^{\mathrm{v}} = \sum_{i=1}^{K-N} (\mathbf{V})_{ik}\mathbf{c}^s \quad (k = 1, ..., N) \tag{16}$$

where $s = N + i$ and $\mathbf{c}^k$ is the k^{th} column of the $\mathbf{C}$ matrix and stores the LCAO coefficients of the k^{th} canonical spin orbital. We also construct[15] the $\mathbf{Y}$ and $\mathbf{Z}$ matrices

$$\mathbf{O}^\dagger\mathbf{T}\mathbf{T}^\dagger\mathbf{O} = \mathbf{Y} \quad (\mathbf{Y})_{ij} = y_i^2\delta_{ij}; \quad \mathbf{V}^\dagger\mathbf{T}^\dagger\mathbf{T}\mathbf{V} = \mathbf{Z} \quad (\mathbf{Z})_{ij} = z_i^2\delta_{ij} \tag{17}$$

When we consider $(K - N) > N$ as it is mostly the case, we see that

$$y_i^2 = z_i^2 \equiv x_i^2 \ \ \forall\ i \subset \{1, N\} \quad z_i^2 = 0 \ \ \forall\ i \subset \{N + 1, K - N\} \tag{18}$$

where x_i comes from eq 15. Note that the previous argument still holds when $N > (K - N)$, but in that case, the first $(K - N)$ x, y, and z values will be nonzero because the SVD will produce $(K - N)$ couples of NTOs rather than N.

From the last three equations, we can express the NTOs in the basis of atomic orbitals

$$\psi_k^{\mathrm{o}}(\xi) = \sum_{i=1}^{K} \varphi_i(\xi)(\mathbf{C}^{\mathrm{o}})_{ik} \quad \psi_k^{\mathrm{v}}(\xi) = \sum_{i=1}^{K} \varphi_i(\xi)(\mathbf{C}^{\mathrm{v}})_{ik} \quad (k = 1, ..., N) \tag{19}$$

where $\mathbf{C}^{\mathrm{o}}$ and $\mathbf{C}^{\mathrm{v}}$ are two $(K \times N)$ matrices storing the NTOs−LCAO coefficients. It is thus possible to define an *occupied* and a *virtual* density matrix derived from the NTOs

$$(\mathbf{P}^{\mathrm{o}})_{ij} = \sum_{l=1}^{N} y_l^2 (\mathbf{C}^{\mathrm{o}})_{il}(\mathbf{C}^{\mathrm{o}})_{jl} \quad (\mathbf{P}^{\mathrm{v}})_{ij} = \sum_{l=1}^{N} z_l^2 (\mathbf{C}^{\mathrm{v}})_{il}(\mathbf{C}^{\mathrm{v}})_{jl} \tag{20}$$

We actually verify that

$$\sum_{i=1}^{K} (\mathbf{P}^{\mathrm{o}}\mathbf{S})_{ii} = \sum_{i=1}^{N} y_i^2 \equiv \sum_{i=1}^{N} z_i^2 = \sum_{i=1}^{K} (\mathbf{P}^{\mathrm{v}}\mathbf{S})_{ii} \tag{21}$$

and

$$\varrho_{\mathrm{X}}(\xi) = \varrho_0(\xi) - \sum_{k=1}^{N} y_k^2 |\psi_k^{\mathrm{o}}(\xi)|^2 + \sum_{k=1}^{N} z_k^2 |\psi_k^{\mathrm{v}}(\xi)|^2 \tag{22}$$

which leads to

$$\varrho_{\mathrm{X}}(\xi) - \varrho_0(\xi) = \varrho_{\mathrm{v}}(\xi) - \varrho_{\mathrm{o}}(\xi) \tag{23}$$

$$\mathbf{P}_{\mathrm{X}} - \mathbf{P}_0 = \mathbf{P}_{\mathrm{v}} - \mathbf{P}_{\mathrm{o}} \tag{24}$$

where $\mathbf{P}_{\mathrm{X}}$ is the unrelaxed X^{th} excited state density matrix ($\mathbf{P}_{\mathrm{o}}$ and $\mathbf{P}_{\mathrm{v}}$ formally correspond to the density matrices representing the hole and the particle, respectively). The last equivalence formally proves that we can use the formerly exposed machinery (i.e., eq 1−4) to obtain the NTOs derived detachment and attachment density matrices, $\mathbf{\Gamma}^{\mathrm{NTO}}$ and

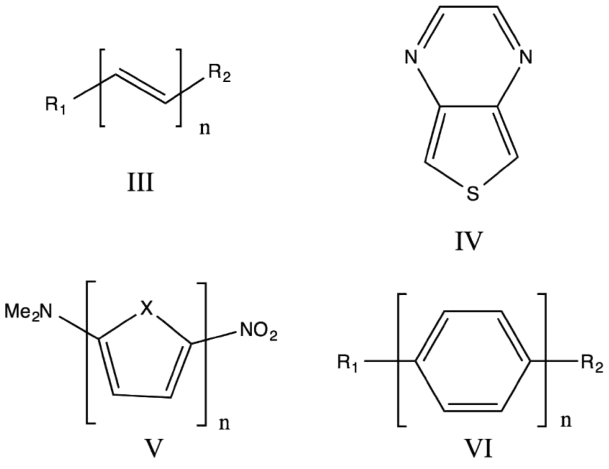

nIII-(c,d) R_1=(NH_2,NMe_2),R_2=NO_2, n=(1,5)	IV See ref [44]
nV-X X=(NH,O,S,Se), n=(1,5)	nVI-c R_1=NMe_2, R_2=NO_2, n=(1,5)

Figure 2. Sketch of the molecules investigated in the present survey.

$\mathbf{\Lambda}^{\mathrm{NTO}}$. These two matrices are therefore exactly identical to the $\mathbf{\Gamma}$ and $\mathbf{\Lambda}$ density matrices of eq 4.

It is now possible to define $\varrho_{\boldsymbol{\tau}}^{\mathrm{NTO}}(\xi)$, $\vartheta_{\boldsymbol{\tau}}^{\mathrm{NTO}}(\xi)$, and $\phi_S^{\mathrm{NTO}}(\xi)$ functions as

$$\varrho_{\boldsymbol{\tau}}^{\mathrm{NTO}}(\xi) = \sum_{\mu=1}^{K}\sum_{\nu=1}^{K}(\boldsymbol{\tau}^{\mathrm{NTO}})_{\mu\nu}\varphi_\mu(\xi)\varphi_\nu^*(\xi)$$
$$\vartheta_\tau^{\mathrm{NTO}} = \int_{\mathbb{R}^3} \mathrm{d}^3\xi\, \varrho_\tau^{\mathrm{NTO}}(\xi) \quad \boldsymbol{\tau} \equiv \mathbf{\Gamma}, \mathbf{\Lambda} \tag{25}$$

and

$$\phi_S^{\mathrm{NTO}} = \vartheta_{\mathrm{NTO}}^{-1}\int_{\mathbb{R}^3}\mathrm{d}^3\xi\sqrt{\varrho_{\mathbf{\Gamma}}^{\mathrm{NTO}}(\xi)\varrho_{\mathbf{\Lambda}}^{\mathrm{NTO}}(\xi)}$$
$$\vartheta_{\mathrm{NTO}} \equiv \frac{1}{2}\left[\int_{\mathbb{R}^3}\mathrm{d}^3\xi\sum_{\tau=\mathbf{\Gamma},\mathbf{\Lambda}}\varrho_\tau^{\mathrm{NTO}}(\xi)\right] \quad \phi_S^{\mathrm{NTO}} \in [0;\,1] \tag{26}$$

We actually see that $\phi_S \equiv \phi_S^{\mathrm{NTO}}$ when condition 24 is verified. This particular result means that from various operators holding a different physical meaning, namely, $\hat{\gamma}$ and $\hat{p}_y = |\mathbf{\Psi}_y\rangle\langle\mathbf{\Psi}_y|$ where y = 0 or X, we can derive exactly the same quantity and consequently characterize an electronic transition's topology with a common tool.

In the particular case where only one couple of NTOs is predominant (as it is mostly the case), we straightforwardly can derive the ϕ_S' index as

$$\phi_S' = \vartheta'^{-1}\int_{\mathbb{R}^3}\mathrm{d}^3\xi\sqrt{|\psi_1^{\mathrm{o}}(\xi)|^2|\psi_1^{\mathrm{v}}(\xi)|^2}$$
$$\vartheta' \equiv \frac{1}{2}\left[\int_{\mathbb{R}^3}\mathrm{d}^3\xi\sum_{\tau=\mathrm{o,v}}|\psi_1^{\tau}(\xi)|^2\right] \quad \phi_S' \in [0;\,1] \tag{27}$$

Note that when this condition is true, the results obtained from detachment/attachment densities are expected to be very close to those deduced from the NTOs-based ϕ_S calculation.

We would like to draw the attention of the reader to the fact that if one uses the Tamm−Dancoff[26] approximation or CIS method for computing electronic transitions of chromophores, it is possible to show that

$$\int_{\mathbb{R}^3}\mathrm{d}^3\xi\varrho_{\mathbf{\Gamma}}^{\mathrm{NTO}}(\xi) = \int_{\mathbb{R}^3}\mathrm{d}^3\xi\varrho_{\mathbf{\Lambda}}^{\mathrm{NTO}}(\xi) = \sum_{k=1}^{K}(\mathbf{\Gamma}^{\mathrm{NTO}}\mathbf{S})_{kk}$$
$$= \sum_{k=1}^{K}(\mathbf{\Lambda}^{\mathrm{NTO}}\mathbf{S})_{kk} = \sum_{i=1}^{N}y_i^2 = \sum_{i=1}^{N}z_i^2 = 1 \tag{28}$$

because no de-excitation is considered within these approaches.

2.3. ϕ_S and λ Descriptor as Diagnostic Tools. As stated in the Introduction, the assessment of the charge-transfer character of an electronic transition constitutes a crucial quantitative diagnostic tool. This tool has been connected with the errors on the TDDFT-computed transition energy in the publication[10] of Peach et al., who suggest the use of a λ descriptor. The latter index is defined as a function of the molecular orbitals involved in the electronic transition and of the **X** and **Y** matrix elements from Casida's equation[28] as

$$\begin{pmatrix}\mathbf{A} & \mathbf{B}\\ \mathbf{B}^* & \mathbf{A}^*\end{pmatrix}\begin{pmatrix}\mathbf{X}\\ \mathbf{Y}\end{pmatrix} = \omega\begin{pmatrix}1 & 0\\ 0 & -1\end{pmatrix}\begin{pmatrix}\mathbf{X}\\ \mathbf{Y}\end{pmatrix}$$
$$\lambda = \left(\sum_{i=1}^{N}\sum_{a=N+1}^{K}(\kappa)_{ia}^2(\mathbf{K})_{ia}\right)\left(\sum_{i=1}^{N}\sum_{a=N+1}^{K}(\kappa)_{ia}^2\right)^{-1} \tag{29}$$

where i and a stand for the occupied and virtual canonical spin orbitals, respectively. In eq 29, we find the following terms

$$(\mathbf{K})_{ia} = \langle|\theta_i\theta_i|\theta_a\theta_a|\rangle; \quad (\kappa)_{ia} = (\mathbf{X})_{ia} + (\mathbf{Y})_{ia} \tag{30}$$

where θ_k is the k^{th} molecular orbital, so that an electronic transition can be pictured as an ensemble of monoexcitations from molecular orbitals i to molecular orbitals a. **X** (**Y**) stores the (de)excitation coefficients and should not be confused with the **X** (**Y**) matrix involved in eq 15 (eq 17, respectively). The λ index takes values ranging from zero to one. The authors relate their descriptor as a diagnostic tool to build a connection between the use of an exchange−correlation functional in LR-TDDFT and the errors on a transition energy computation, depending on whether this transition has a local, charge-transfer, or Rydberg character. We will show that the use of the

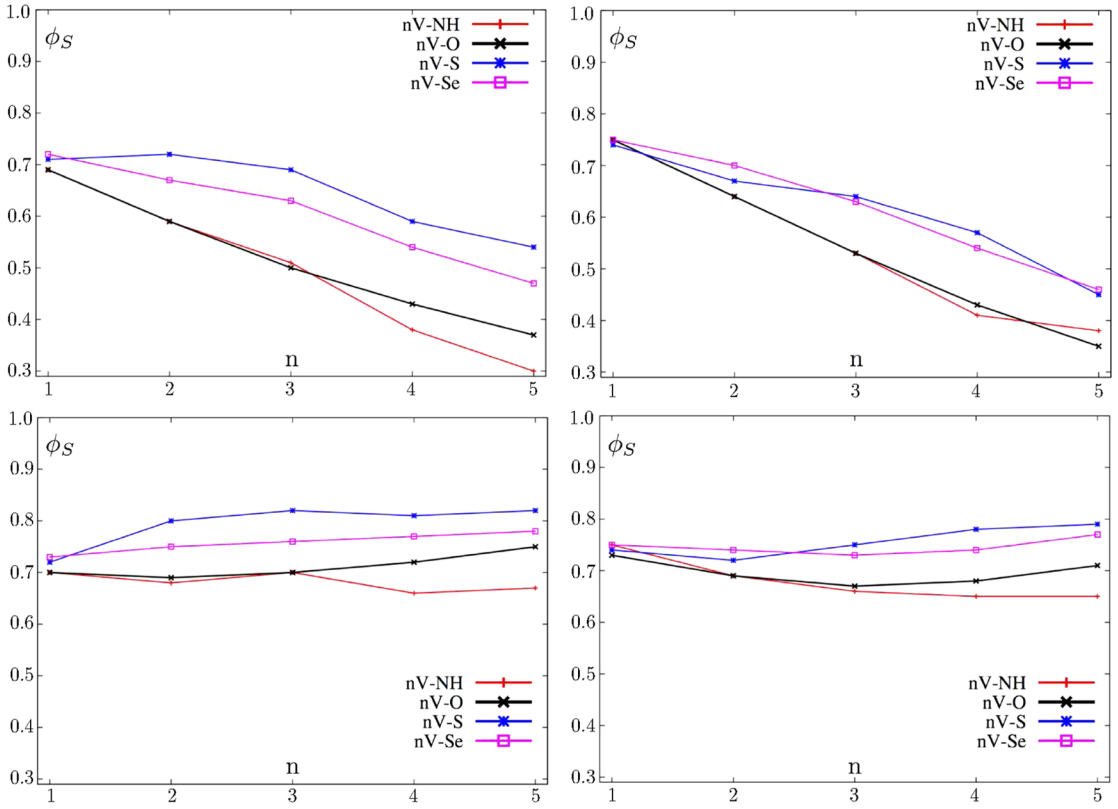

Figure 3. Plot of the ϕ_S index values as a function of n for the nV-X chromophores' first transitions computed with B3LYP in vacuum (top left) or in acetonitrile (top right) and CAM-B3LYP in vacuum (bottom left) or in acetonitrile (bottom right).

λ index can be compared to the one for ϕ_S for a diagnostic purpose despite different formal definitions.

2.4. Computational Strategy. All DFT and nonequilibrium linear-response TDDFT calculations were performed using the Gaussian 09 (revision B01) package.[29] For the first set of molecules (III, V, and VI derivatives; Figure 2), geometries were computed using the PBE0/6-311G(d,p) level of theory[30−32] with tight convergence criteria imposed both on the self-consistent field (residual mean square is 10^{-9} a.u.) and on geometry optimization (residual mean square force threshold is 10^{-5} a.u.), which is known to provide reliable geometries for organic compounds. Frequency calculations were done for equilibrium geometries with the same level of theory to confirm that the optimized geometries are true minima of the potential energy surface. Excited states were computed within the Franck−Condon principle stating that all the electronic excitations are vertical. Various exchange−correlation functionals were used for this purpose, namely, the parameter-free PBE0, hybrid B3LYP,[33,34] and range-separated CAM-B3LYP[35] xc-functionals together with the 6-311++G(2d,p) basis set[32] (except for the second test set, see below). This choice of functionals allows us to address issues relative to the use of a parameter-free functional with respect to a parametrized one and more importantly the comparison between a hybrid functional and its long-range corrected version. Because B3LYP is known to overestimate the charge-transfer, it is clearly expected to give lower ϕ_S indices as compared to those from CAM-B3LYP for a same set of molecules. Solvation was accounted for by a self-consistent reaction field[36] (SCRF) thanks to the integral equation formalism[37,38] (IEF) of the polarizable continuum model[36] (PCM). The cavitation model used requires the universal force field cavitation energies and atomic radii. Acetonitrile solvent was used throughout.

As an illustrative example, we will assess the ϕ_S index for a set of α,ω-NMe_2,NO_2 molecules with terminal fragments spaced by double bonds (III dyes), phenyles (VI dyes), thiophenes, pyrroles, furanes, or selenophenes (nV-X dyes). The number n of spacer subunits ranges from 1 to 5 for each subset. Most of these chromophores were previously studied by Ciofini et al.[39,40] using the barycenter approach.[41−44,47]

The core of the present investigation is devoted to a quantitative assessment of the specific influence of using different spacers, as well as the use of various number of bridge subunits and the presence/absence of solvation together with the level of theory in use. Indeed, we will focus on the influence of the spacers' size extension and the choice of the heteroatom with respect to the computed photoinduced charge separation or conversely to the importance of the detachment/attachment overlap because a low overlap corresponds to an important charge-transfer. Furthermore, the choice of hybrid or range-separated exchange−correlation functional will be connected to the ϕ_S trends. All the calculations from the first set of molecules were also performed in vacuum to assess the solvation contribution to the ϕ_S trends.

The second test set was previously studied by Jacquemin et al.[44] with the help of centroid-based characterization. It consists in a set of 36 thieno[3,4-*b*]pyrazines derivatives. The core fragment is recalled in Figure 2 (molecule IV). The molecular set was computed separately using the level of theory reported in ref 44, i.e., CAM-B3LYP/6-311+G(2d,p)//PBE0/6-311G-(d,p). Acetonitrile solvation effects were also modeled by IEF−PCM. Six electronic transitions were computed for each of these molecules, and natural transition orbitals as well as

dx.doi.org/10.1021/ct5003994 | J. Chem. Theory Comput. 2014, 10, 3896−3905

detachment/attachment densities were obtained. When only one couple of NTOs prevailed, ϕ_S, ϕ'_S, and ϕ_S^{NTO} values were compared.

Finally, the molecular set from Peach et al.[10,11] was taken into account. We reproduced the calculations reported in ref 10 and analyzed the errors on excitation energies with respect to the ϕ_S descriptor value. Hence the possibility to use ϕ_S index as a diagnostic tool will be further discussed in parallel with the common use of so-called λ index.[10,11]

All the detachment/attachment densities, natural transition orbitals, and ϕ_S indices were computed using a homemade code developed in our laboratory.[45] Its use consists in a post-processing of the Gaussian 09 package, together with the use of the Cubegen[29] utility to generate the tridimensional integration grids.

3. RESULTS

Detailed numerical results related to the molecules from Figure 2 (ϕ_S index, excitation energies, and oscillator strengths) are all reported in the Supporting Information. Figure 3 depicts the ϕ_S trends as a function of the number of subunits in the *n*V-X subset of molecules, computed with B3LYP and CAM-B3LYP in vacuum and in acetonitrile. It clearly appears, as expected, because B3LYP is known to systematically overestimate the charge-transfer, that ϕ_S values are significantly lower with this xc-functional than with CAM-B3LYP. A qualitative depiction of the difference between B3LYP and CAM-B3LYP results is reported in Figure S1 of the Supporting Information where the detachment/attachment density plot in the direct space shows that the first transition of 5 V−S has a stronger charge-transfer character when computed with B3LYP than with CAM-B3LYP. Furthermore, one can notice an evident saturation of the ϕ_S value with CAM-B3LYP, which actually means that the range-separation correction of this xc-functional leads to a lower fluctuation of the ϕ_S magnitude with respect to the spatial extension of the π-conjugated bridge. This feature leads to more physically sounding results because one can obviously expect a saturation in the charge-transfer when the distance between the hole and particle becomes too large. CAM-B3LYP can also be viewed as underestimating CT, which can be compared with the known CAM-B3LYP hyperpolarizability underestimation.[49] It has however to be noted that such underestimation will take place only for a large spatial extent of the CT, i.e., only in the case of a large number of bridging subunits, *n*.[46] This behavior is of course not reproduced by B3LYP and PBE0 (which unsurprisingly give quite close results) for the previously cited reason. Hence, in the latter case, the trend is a net decrease in ϕ_S when the molecular size increases. Interestingly, we notice the split of the *n*V-X subset into two classes, oligopyrrole and oligofurane, form a subset with lower ϕ_S than oligothiophene and oligoselenophene. On the other hand, both groups of molecules are shown to have a closer ϕ_S values when acetonitrile solvation effects are accounted for (see the right part of Figure 3). Moreover, solvent effects have also consequences on the absolute value of ϕ_S, which tends to be systematically slightly lower in acetonitrile than in vacuum. Our conclusions can therefore be regarded as complementary to those drawn in ref 39 by Ciofini et al. (revealing an increase in the charge-transfer distance and of the amount of transferred charge with respect to the number of spacer subunits) from a different theoretical approach.

*n*VI-c molecular set equivalently behaves when its spacer size is augmented (Figure 4) but with a significantly lower extreme

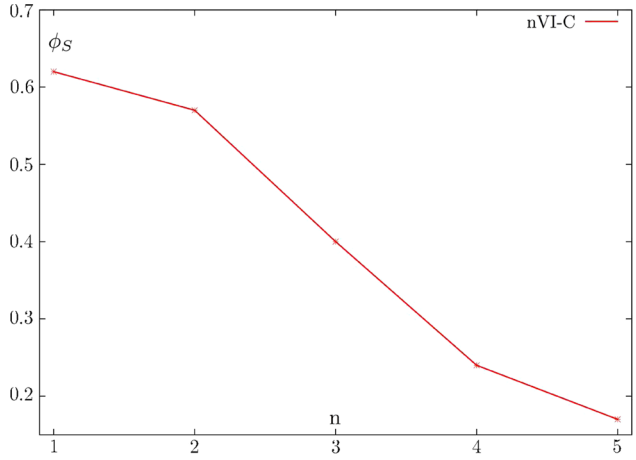

Figure 4. Plot of the ϕ_S index values as a function of *n* for the *n*VI-c chromophores' first transitions in acetonitrile computed with PBE0/6-311++G(2d,p).

ϕ_S value (0.17) for $n = 5$ with PBE0 in acetonitrile, denoting a longer-ranged charge-transfer, as depicted in Figure 5 in which we report illustratively the detachment and attachment densities of the 5VI-c molecule.

Unlike the previously cited systems, if the spacer is an oligoene, the variation of ϕ_S with respect to the number of spacer subunits has a much weaker magnitude than in previous sets. This leads us to the conclusion that such a spacer is much less sensitive to an increase in its size extension, as reported in Table 1. A possible explanation could rise from the fact that conjugation is higher in oligoene-bridged systems due to the planarity of the structures. Hence, the communication between donor and acceptor functions is increased in the case of the *n*III-c subset, which makes the detachment/attachment densities overlap higher. Hence, ϕ_S values are unsurprisingly higher for these compounds, without regard to the number of spacer subunits.

The same computation as before was performed on the *n*V-S chromophores subset but with second-order excited states electron densities (i.e., when the linear-response density is relaxed in order to take into account electron density reorganization effects). Despite the fact that the overall trends are correctly reproduced, the respective values of ϕ_S are too tightly ranged due to higher ϑ values, which means that no sounding analysis can be derived from such a topological analysis.

Figure 6 consists in two plots. The blue dots depict the comparison between the ϕ_S and ϕ_S^{NTO} values, while the red dots plot displays the relationship between ϕ_S and ϕ'_S (where one couple of NTOs is considered). Values are obtained from the IV subset (see the Computational Strategy section and ref 44) where we selected transitions in which one couple of NTOs prevailed for the sake of comparison between ϕ_S^{NTO} and the one-couple ϕ'_S approximation. The results are given in Figure 6 and are detailed in the Supporting Information. We see that while ϕ'_S already constitutes a reliable approximation to ϕ_S (R^2 is 0.991), the ϕ_S^{NTO} index can be considered as identical to ϕ_S (R^2 is 0.997), which proves that the obtention of our descriptor from these two various approaches is undoubtly equivalent, up to any possible numerical error.

Finally, we reproduced the computation of transition energies of the Peach et al. set of molecules.[10] The resulting plot (Figure 7) of the errors on a transition energy with respect

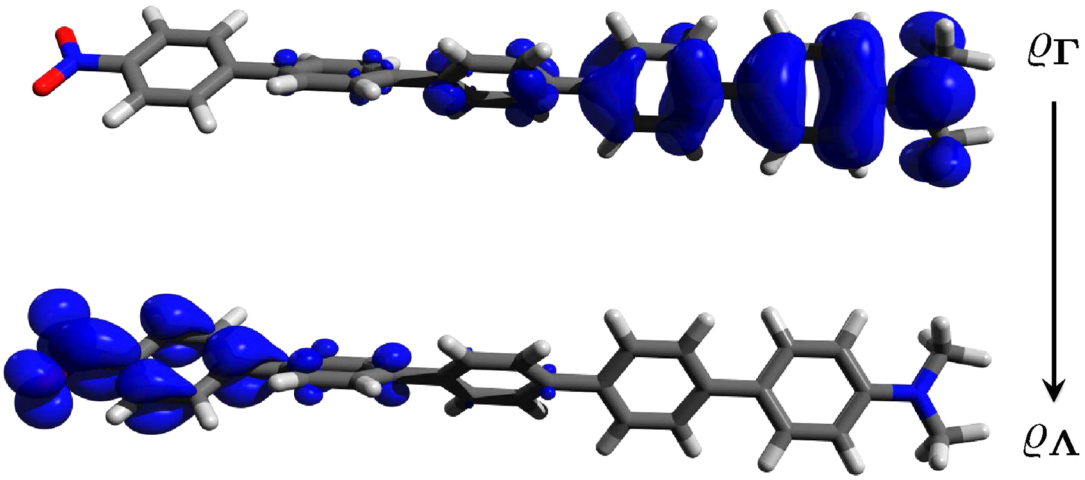

Figure 5. Example of a long-range charge-transfer for the 5VI-c molecule's first transition in acetonitrile computed with PBE0/6-311++G(2d,p).

Table 1. *n*III-c ϕ_S Trend, Computed in Acetonitrile with B3LYP/6-311++G(2d,p) Level of Theory[a]

no.	t	λ	f	ϕ_S
1III-c	2	285.17	0.4385	0.68
2III-c	1	349.57	0.8489	0.69
3III-c	1	412.60	1.2813	0.69
4III-c	1	473.85	1.7053	0.69
5III-c	1	534.59	2.1000	0.69

[a] t is the number of the transition computed, λ is the transition wavelength (nm), and f is the oscillator strength associated to the t^{th} transition.

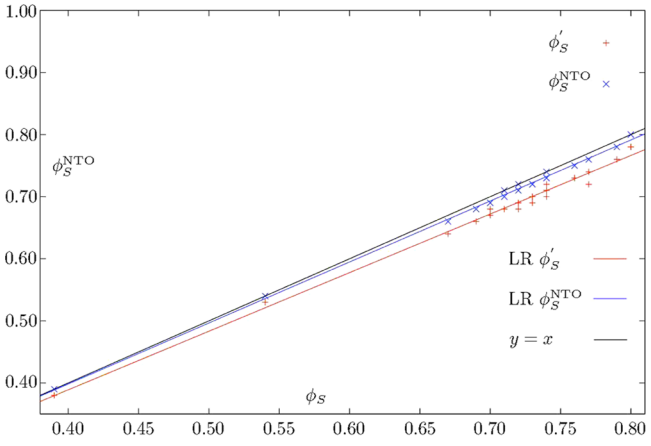

Figure 6. Comparison of the original ϕ_S with its NTOs derivation for the IV-based molecules for which one couple of NTOs prevailed. General definition of the NTOs derived detachment/attachment densities ($\phi_S^{NTO} = 0.982\phi_S + 0.005$; blue dots) is compared to the use of the one-couple approximation ($\phi'_S = 0.944\phi_S + 0.012$; red dots), together with their linear regressions (LR). R^2 values are 0.991 for ϕ'_S and 0.997 for ϕ_S^{NTO}. Black line is the $y = x$ function.

to the ϕ_S values using the PBE,[48] B3LYP, and CAM-B3LYP xc-functionals shows exactly the same trends as one found in ref 10. We can therefore state that our new descriptor can be used as a diagnostic tool for the assessment of the charge-transfer character of a molecule, equivalent to the λ index. Nevertheless, one should be aware of the fact that the ϕ_S and λ descriptors arise from different theoretical foundations. It is also important to point here that consistently with the λ index approach if the

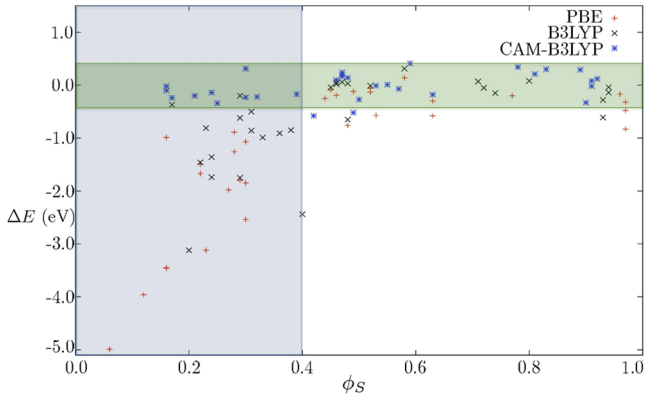

Figure 7. Plot of the error on excitation energies (in eV) as a function of the ϕ_S descriptor applied to the Peach et al.[10] test set with various functional usages. The typical error associated with TDDFT is comprised inside the horizontal green area. Left blue area is associated with a small overlap between detachment and attachment densities ($\phi_S < 0.4$) and indicates that a range-separated functional is required.

ϕ_S descriptor value is lower than 0.4 (blue rectangle in Figure 7) then the PBE and B3LYP xc-functionals will lead to high errors in the transition energy. Only the use of long-range corrected functionals such as CAM-B3LYP reduces errors for low ϕ_S (lower than 0.4) regions to acceptable errors. On the other hand, if the ϕ_S index value is higher than 0.4 all the functionals give excitation energies close to the commonly accepted TDDFT error bar of ±0.2 eV (green rectangle in Figure 7).

4. CONCLUSION

The mathematical background of the ϕ_S index construction has been detailed. Its calculation for a large set of molecules with variable structure has been performed within various levels of theory. It especially appeared that this model can be useful for retrieving informations on the excited states of various chromophores and of their charge-transfer character. These molecular targets can constitute potential candidates for different optoelectronic applications as well as for energy production as in dye-sensitized solar cells (donor−π−acceptor dyes). A second possible derivation of the ϕ_S descriptor was exposed and validated by quantum chemical calculations. Furthermore, we demonstrated that the theoretical foundations

of our new descriptor are physically sounding and that its assessment can provide an interesting insight into the photophysics of chromophores. Moreover, this simple approach also allows us to address a comment relative to the behavior of an exchange−correlation functional with respect to the charge-transfer character of a molecule. Thus, its use as a diagnostic tool has been validated. From these results, we could clearly evidence similarities between our new approach and the formerly developed λ descriptor despite some existing discrepancies between the two approaches' theoretical foundations. From this investigation, we can conclude that the ϕ_S index constitutes an interesting instrument for the computation of electronic properties of dyes because the following: (i) It quantitatively characterizes the charge-transfer character of an electronic transition. (ii) Its nonexpensive computation constitutes an xc-functional diagnostic test. (iii) Natural transition orbitals can provide a graphical depiction of the excited state topology and can also be used for ϕ_S computation.

Finally, its computation could be exploited complementarily to other approaches in order to probe the potentiality of new chromophores, or simply to explain the photoactivity of existing dyes according to experimental data.

APPENDIX A. TRANSITION DENSITY MATRIX FROM THE SECOND QUANTIZATION

We demonstrate here that eq 14 can equivalently be derived from the use of second quantization through creation/anihilation operators. We define

$$(\mathbf{T})_{mn} = \langle \mathbf{\Psi}_0 | \hat{a}_m^\dagger \hat{a}_p | \mathbf{\Psi}_X \rangle \tag{31}$$

where again we used the rule $p = N + n$. If the excited state can be written as an expansion over the space of monoexcited Slater determinants, we have

$$|\mathbf{\Psi}_X\rangle = \sum_{i=1}^{N} \sum_{a=N+1}^{K} c_i^a |\mathbf{\Psi}_i^a\rangle \tag{32}$$

hence leading to

$$(\mathbf{T})_{mn} = \sum_{i=1}^{N} \sum_{a=N+1}^{K} c_i^a \langle \mathbf{\Psi}_0 | \hat{a}_m^\dagger \hat{a}_p | \mathbf{\Psi}_i^a \rangle \tag{33}$$

The action of anihilation $\hat{a}_m^\dagger$ and creation $\hat{a}_p$ operators on the bra $\langle \mathbf{\Psi}_0|$ leads to

$$(\mathbf{T})_{mn} = \sum_{i=1}^{N} \sum_{a=N+1}^{K} c_i^a \langle \mathbf{\Psi}_m^p | \mathbf{\Psi}_i^a \rangle = c_m^p \delta_{im} \delta_{ap} = c_m^p \tag{34}$$

which corresponds to our deduction of eq 14.

APPENDIX B. SINGULAR VALUE DECOMPOSITION OF THE TRANSITION DENSITY MATRIX

This paragraph contains a new definition of the natural transition orbitals. This derivation involves a singular value decomposition of the transition density matrix performed in the space of canonical spin orbitals rather than in the molecular orbitals space. The use of molecular orbitals for this sake has been formerly exposed in details by Mayer in ref 17. We show here that using the spin orbitals space allows a straightforward analysis of excited states topology with a common strategy for (un)restricted calculations.

Thanks to the definition of the $\mathbf{T}$ matrix given in eq 14 and 34 we have

$$\begin{aligned} \mathbf{\Psi}_{ex} &= \sum_{i=1}^{N} \sum_{a=N+1}^{K} c_i^a \hat{a}_a^\dagger \hat{a}_i |\mathbf{\Psi}_0\rangle = \sum_{m=1}^{N} \sum_{n=1}^{K-N} c_m^p \hat{a}_p^\dagger \hat{a}_m |\mathbf{\Psi}_0\rangle \\ &= \sum_{m=1}^{N} \sum_{n=1}^{K-N} (\mathbf{T})_{mn} \hat{a}_p^\dagger \hat{a}_m |\mathbf{\Psi}_0\rangle \quad (p = N + n) \end{aligned} \tag{35}$$

one can rewrite the $(N \times [K - N])$ $\mathbf{T}$ matrix

$$\mathbf{T} = \mathbf{1}^o \mathbf{T} \mathbf{1}^v \tag{36}$$

with

$$\mathbf{1}^o (N \times N) | (\mathbf{1}^o)_{ij} = \delta_{ij} \quad \mathbf{1}^v ([K - N] \times [K - N]) | (\mathbf{1}^v)_{ij} = \delta_{ij} \tag{37}$$

and define the unit matrices $\mathbf{1}^o$ and $\mathbf{1}^v$ by the product of a unitary matrix and its adjoint

$$\mathbf{1}^o = \mathbf{O}\mathbf{O}^\dagger, \ \mathbf{1}^v = \mathbf{V}\mathbf{V}^\dagger \Rightarrow \mathbf{T} = \mathbf{O}\mathbf{O}^\dagger \mathbf{T} \mathbf{V}\mathbf{V}^\dagger \tag{38}$$

We define the diagonal $\mathbf{X}$ matrix as

$$\mathbf{X} = \mathbf{O}^\dagger \mathbf{T} \mathbf{V} \Leftrightarrow \mathbf{T} = \mathbf{O}\mathbf{X}\mathbf{V}^\dagger \tag{39}$$

The components of $\mathbf{T}$, thanks to its latter definition, are

$$(\mathbf{T})_{mn} = \sum_{q=1}^{N} \sum_{r=1}^{K-N} (\mathbf{O})_{mq} (\mathbf{X})_{qr} (\mathbf{V}^\dagger)_{rn} \tag{40}$$

If we impose $\mathbf{V}$ to be real,

$$(\mathbf{V})_{kl} \in \mathbb{R} \Rightarrow (\mathbf{T})_{mn} = \sum_{q=1}^{N} \sum_{r=1}^{K-N} (\mathbf{O})_{mq} (\mathbf{X})_{qr} (\mathbf{V})_{nr} \tag{41}$$

We can therefore rewrite 35

$$|\mathbf{\Psi}_{ex}\rangle = \sum_{n=1}^{K-N} \sum_{m=1}^{N} \sum_{r=1}^{K-N} \sum_{q=1}^{N} (\mathbf{X})_{qr} [(\mathbf{V})_{nr} \hat{a}_p^\dagger] [(\mathbf{O})_{mq} \hat{a}_m] | \mathbf{\Psi}_0 \rangle \quad (p = N + n) \tag{42}$$

and define the ψ_k^o and ψ_k^v functions with respect to the corresponding creation/annihilation operators and the spin orbitals Θ_i, considering $N < K - N$

$$\psi_k^o = \sum_{i=1}^{N} (\mathbf{O})_{ik} c^i \quad \left(\hat{\psi}_k^o = \sum_{i=1}^{N} (\mathbf{O})_{ik} \hat{a}_i \right) \quad (k = 1, \ldots, N) \tag{43}$$

and

$$\psi_k^v = \sum_{i=1}^{K-N} (\mathbf{V})_{ik} c^s \quad \left(\hat{\psi}_k^{v\dagger} = \sum_{i=1}^{K-N} (\mathbf{V})_{ik} \hat{a}_s^\dagger \right) \quad (k = 1, \ldots, N) \tag{44}$$

where $s = N + i$ and $\mathbf{c}^k$ is the k^{th} column of the $\mathbf{C}$ matrix, so that $\mathbf{c}^k$ stores the LCAO coefficients of the k^{th} canonical spin orbital. Actually, we can rewrite the last equation as

$$(\mathbf{X})_{ij} = x_i \delta_{ij} \Rightarrow |\mathbf{\Psi}_{ex}\rangle = \sum_{k=1}^{N} x_k \hat{\psi}_k^{v\dagger} \hat{\psi}_k^o |\mathbf{\Psi}_0\rangle \tag{45}$$

dx.doi.org/10.1021/ct5003994 | J. Chem. Theory Comput. 2014, 10, 3896−3905

where k stands for the k^{th} couple of occupied (o) and virtual (v) natural transition orbitals ψ_k^o and ψ_k^v. Those couples are ordered by decreasing values of x_k.

■ ASSOCIATED CONTENT

Supporting Information

Transition wavelength, oscillator strength, and ϕ_S index values for PBE0, B3LYP, and CAM-B3LYP in vacuum and acetonitrile. ϕ_S index values from detachment/attachment and NTOs density matrices and one-couple NTOs densities. Qualitative comparison of the charge-transfer character of 5 V−S with B3LYP and CAM-B3LYP. This material is available free of charge via the Internet at http://pubs.acs.org.

■ AUTHOR INFORMATION

Corresponding Author

*E-mail: thibaud.etienne@univ-lorraine.fr.

Notes

The authors declare no competing financial interest.

■ ACKNOWLEDGMENTS

A.M. thanks CNRS for funding the "chaire d'excellence" project. All the authors are very grateful to the PhiScience Association for its valuable activity. Dr. Thibaut Very is acknowledged for his contribution to the development of the NANCY_EX software suite. We also acknowledge support from the "Balance Supra" ANR project.

■ REFERENCES

(1) Labat, F.; Le Bahers, T.; Ciofini, I.; Adamo, C. First-principles modeling of dye-sensitized solar cells: Challenges and perspectives. *Acc. Chem. Res.* **2012**, *45*, 1268−1277.

(2) Le Bahers, T.; Pauporté, T.; Lainé, P. P.; Labat, F.; Adamo, C.; Ciofini, I. Modeling dye-sensitized solar cells: From theory to experiment. *J. Phys. Chem. Lett.* **2013**, *4*, 1044−1050.

(3) Hagfeldt, A.; Grätzel, M. Molecular photovoltaics. *Acc. Chem. Res.* **2000**, *33*, 269−277.

(4) Preat, J.; Hagfeldt, A.; Perpète, E. A. Investigation of the photoinduced electron injection processes for p-type triphenylamine-sensitized solar cells. *Energy Environ. Sci.* **2011**, *4*, 4537−4549.

(5) Etienne, T.; Chbibi, L.; Michaux, C.; Perpète, E. A.; Assfeld, X.; Monari, A. All-organic chromophores for dye-sensitized solar cells: A theoretical study on aggregation. *Dyes Pigm.* **2014**, *101*, 203−211.

(6) Preat, J.; Michaux, C.; Jacquemin, D.; Perpète, E. A. Enhanced efficiency of organic dye-sensitized solar cells: Triphenylamine derivatives. *J. Phys. Chem. C* **2009**, *113*, 16821−16833.

(7) Tang, J.; Qu, S.; Hu, J.; Wu, W.; Hua, J. A new organic dye bearing aldehyde electron-withdrawing group for dye-sensitized solar cell. *Sol. Energy* **2012**, *86*, 2306−2311.

(8) Guido, C. A.; Cortona, P.; Mennucci, B.; Adamo, C. On the metric of charge transfer molecular excitations: A simple chemical descriptor. *J. Chem. Theory Comput.* **2013**, *9*, 3118−3126.

(9) Guido, C. A.; Cortona, P.; Adamo, C. Effective electron displacements: A tool for time-dependent density functional theory computational spectroscopy. *J. Chem. Phys.* **2014**, *140*, 104101.

(10) Peach, M. J. G.; Benfield, P.; Helgaker, T.; Tozer, D. J. Excitation energies in density functional theory: An evaluation and a diagnostic test. *J. Chem. Phys.* **2008**, *128*, 044118−044118−8.

(11) Peach, M. J. G.; Sueur, C. R. L.; Ruud, K.; Guillaume, M.; Tozer, D. J. TDDFT diagnostic testing and functional assessment for triazene chromophores. *Phys. Chem. Chem. Phys.* **2009**, *11*, 4465−4470.

(12) Monari, A.; Assfeld, X.; Beley, M.; Gros, P. C. Theoretical study of new ruthenium-based dyes for dye-sensitized solar cells. *J. Phys. Chem. A* **2011**, *115*, 3596−3603.

(13) Dreuw, A.; Head-Gordon, M. Single-reference ab initio methods for the calculation of excited states of large molecules. *Chem. Rev.* **2005**, *105*, 4009−4037.

(14) Luzanov, A. V.; Sukhorukov, A. A.; Umanskii, V.É. Application of transition density matrix for analysis of excited states. *Theor. Exp. Chem.* **1976**, *10*, 354−361.

(15) Martin, R. L. Natural transition orbitals. *J. Chem. Phys.* **2003**, *118*, 4775−4777.

(16) Batista, E. R.; Martin, R. L. Natural Transition Orbitals. In *Encyclopedia of Computational Chemistry*; John Wiley & Sons, Ltd.: New York, **2004**.

(17) Mayer, I. Using singular value decomposition for a compact presentation and improved interpretation of the CIS wave functions. *Chem. Phys. Lett.* **2007**, *437*, 284−286.

(18) Mayer, I. Identifying a pair of interacting chromophores by using SVD transformed CIS wave functions. *Chem. Phys. Lett.* **2007**, *443*, 420−425.

(19) Very, T.; Despax, S.; Hébraud, P.; Monari, A.; Assfeld, X. Spectral properties of polypyridyl ruthenium complexes intercalated in DNA: Theoretical insights into the surrounding effects of [Ru(dppz)-(bpy)2]2+. *Phys. Chem. Chem. Phys.* **2012**, *14*, 12496−12504.

(20) Chantzis, A.; Very, T.; Daniel, C.; Monari, A.; Assfeld, X. Theoretical evidence of photo-induced charge transfer from DNA to intercalated ruthenium (II) organometallic complexes. *Chem. Phys. Lett.* **2013**, *578*, 133−137.

(21) Lachaud, F.; Jeandon, C.; Monari, A.; Assfeld, X.; Beley, M.; Ruppert, R.; Gros, P. C. New dyads using (metallo)porphyrins as ancillary ligands in polypyridine ruthenium complexes. Synthesis and electronic properties. *Dalton Trans.* **2012**, *41*, 12865−12871.

(22) Chantzis, A.; Very, T.; Monari, A.; Assfeld, X. Improved treatment of surrounding effects: UV/vis absorption properties of a solvated Ru(II) complex. *J. Chem. Theory Comput.* **2012**, *8*, 1536−1541.

(23) Lachaud, F.; Jeandon, C.; Beley, M.; Ruppert, R.; Gros, P. C.; Monari, A.; Assfeld, X. Ground and excited state properties of new porphyrin based dyads: A combined theoretical and experimental study. *J. Phys. Chem. A* **2012**, *116*, 10736−10744.

(24) Monari, A.; Very, T.; Rivail, J.-L.; Assfeld, X. A QM/MM study on the spinach plastocyanin: Redox properties and absorption spectra. *Comput. Theor. Chem.* **2012**, *990*, 119−125.

(25) Etienne, T.; Michaux, C.; Monari, A.; Assfeld, X.; Perpète, E. A. Theoretical computation of Betain B30 solvatochromism using a polarizable continuum model. *Dyes Pigm.* **2014**, *100*, 24−31.

(26) Chantzis, A.; Laurent, A. D.; Adamo, C.; Jacquemin, D. Is the Tamm-Dancoff approximation reliable for the calculation of absorption and fluorescence band shapes? *J. Chem. Theory Comput.* **2013**, *9*, 4517−4525.

(27) Amos, A. T.; Hall, G. G. Single determinant wave functions. *Proc. R. Soc. London; Ser. A* **1961**, *263*, 483−493.

(28) Casida, M. E. Time-dependent density-functional theory for molecules and molecular solids. *J. Mol. Struct.: THEOCHEM* **2009**, *914*, 3−18.

(29) Frisch, M. J.; Trucks, G. W.; Schlegel, H. B.; Scuseria, G. E.; Robb, M. A.; Cheeseman, J. R.; Scalmani, G.; Barone, V.; Mennucci, B.; Petersson, G. A.; Nakatsuji, H.; Caricato, M.; Li, X.; Hratchian, H. P.; Izmaylov, A. F.; Bloino, J.; Zheng, G.; Sonnenberg, J. L.; Hada, M.; Ehara, M.; Toyota, K.; Fukuda, R.; Hasegawa, J.; Ishida, M.; Nakajima, T.; Honda, Y.; Kitao, O.; Nakai, H.; Vreven, T.; Montgomery, J. A.; , Jr., Peralta, J. E.; Ogliaro, F.; Bearpark, M.; Heyd, J. J.; Brothers, E.; Kudin, K. N.; Staroverov, V. N.; Keith, T.; Kobayashi, R.; Normand, J.; Raghavachari, K.; Rendell, A.; Burant, J. C.; Iyengar, S. S.; Tomasi, J.; Cossi, M.; Rega, N.; Millam, J. M.; Klene, M.; Knox, J. E.; Cross, J. B.; Bakken, V.; Adamo, C.; Jaramillo, J.; Gomperts, R.; Stratmann, R. E.; Yazyev, O.; Austin, A. J.; Cammi, R.; Pomelli, C.; Ochterski, J. W.; Martin, R. L.; Morokuma, K.; Zakrzewski, V. G.; Voth, G. A.; Salvador, P.; Dannenberg, J. J.; Dapprich, S.; Daniels, A. D.; Farkas, O.; Foresman, J. B.; Ortiz, J. V.; Cioslowski, J.; Fox, D. J. *Gaussian 09*, revision B.01, Gaussian, Inc.: Wallingford, CT, 2010.

(30) Adamo, C.; Barone, V. Toward reliable density functional methods without adjustable parameters: The PBE0 model. *J. Chem. Phys.* **1999**, *110*, 6158−6170.
(31) Adamo, C.; Scuseria, G. E.; Barone, V. Accurate excitation energies from time-dependent density functional theory: Assessing the PBE0 model. *J. Chem. Phys.* **1999**, *111*, 2889−2899.
(32) Frisch, M. J.; Pople, J. A.; Binkley, J. S. Self-consistent molecular orbital methods 25. Supplementary functions for Gaussian basis sets. *J. Chem. Phys.* **1984**, *80*, 3265−3269.
(33) Becke, A. D. Density-functional thermochemistry. III. The role of exact exchange. *J. Chem. Phys.* **1993**, *98*, 5648−5652.
(34) Lee, C.; Yang, W.; Parr, R. G. Development of the Colle−Salvetti correlation-energy formula into a functional of the electron density. *Phys. Rev. B* **1988**, *37*, 785−789.
(35) Yanai, T.; Tew, D. P.; Handy, N. C. A new hybrid exchange-correlation functional using the Coulomb-attenuating method (CAM-B3LYP). *Chem. Phys. Lett.* **2004**, *393*, 51−57.
(36) Tomasi, J.; Mennucci, B.; Cammi, R. Quantum mechanical continuum solvation models. *Chem. Rev.* **2005**, *105*, 2999−3094.
(37) Cancès, E.; Mennucci, B.; Tomasi, J. A new integral equation formalism for the polarizable continuum model: Theoretical background and applications to isotropic and anisotropic dielectrics. *J. Chem. Phys.* **1997**, *107*, 3032−3041.
(38) Mennucci, B.; Cancès, E.; Tomasi, J. Evaluation of solvent effects in isotropic and anisotropic dielectrics and in ionic solutions with a unified integral equation method: Theoretical bases, computational implementation, and numerical applications. *J. Phys. Chem. B* **1997**, *101*, 10506−10517.
(39) Ciofini, I.; Le Bahers, T.; Adamo, C.; Odobel, F.; Jacquemin, D. Through-space charge transfer in rod-like molecules: Lessons from theory. *J. Phys. Chem. C* **2012**, *116*, 11946−11955.
(40) Ciofini, I.; Le Bahers, T.; Adamo, C.; Odobel, F.; Jacquemin, D. Correction to "Through-space charge transfer in rod-like molecules: Lessons from theory. *J. Phys. Chem. C* **2012**, *116*, 14736−14736.
(41) Le Bahers, T.; Adamo, C.; Ciofini, I. A qualitative index of spatial extent in charge-transfer excitations. *J. Chem. Theory Comput.* **2011**, *7*, 2498−2506.
(42) Garcia, G.; Adamo, C.; Ciofini, I. Evaluating push−pull dye efficiency using TD-DFT and charge transfer indices. *Phys. Chem. Chem. Phys.* **2013**, *15*, 20210−20219.
(43) Jacquemin, D.; Le Bahers, T.; Adamo, C.; Ciofini, I. What is the "best" atomic charge model to describe through-space charge-transfer excitations? *Phys. Chem. Chem. Phys.* **2012**, *14*, 5383−5388.
(44) Céron-Carrasco, J. P.; Siard, A.; Jacquemin, D. Spectral signatures of thieno[3,4-b]pyrazines: Theoretical interpretations and design of improved structures. *Dyes Pigm.* **2013**, *99*, 972−978.
(45) NAncy-EX. http://nancyex.sourceforge.net (accessed June 13, 2014).
(46) Sun, H.; Autschbach, J. Influence of the delocalization error and applicability of optimal functional tuning in density functional calculations of nonlinear optical properties of organic donor-acceptor chromophores. *ChemPhysChem* **2013**, *14*, 2450−2461.
(47) Etienne, T.; Assfeld, X.; Monari, A. New insight into the topology of excited states through detachment/attachment density matrices-based centroids of charge. *J. Chem. Theory Comput.* **2014**, DOI: 10.1021/ct500400s.
(48) Perdew, J. P.; Burke, K.; Ernzerhof, M. Generalized gradient approximation made simple. *Phys. Rev. Lett.* **1996**, *77*, 3865.
(49) Day, P. N.; Pachter, R.; Nguyen, K. A. Analysis of nonlinear optical properties in donor-acceptor materials. *J. Chem. Phys.* **2014**, *140*, 184308.